The STAR Barrel Electromagnetic Calorimeter

M. Beddo[a], E. Bielick[a], T. Fornek[a], V. Guarino[a], D. Hill[a], K. Krueger[a],
T. LeCompte[a], D. Lopiano[a], H. Spinka[a], D. Underwood[a], A. Yokosawa[a],
R. Brown[b], W. Christie[b], T. Hallman[b], T. Ljubicic[b], D. Padrazo[b], Yu.I. Ivanshin[c],
I.A. Savin[c], V.S. Shvetsov[c], R.Ya. Zulkarneev[c], J. Balewski[d], L.C. Bland[d],
W. Hunt[d], W.W. Jacobs[d], A. Klyachko[d], M. Planinic[d], S. Razin[d], T. Rinckel[d],
K.A. Solberg[d], J. Sowinski[d], E.J. Stephensen[d], S.E. Vigdor[d], S.W. Wissink[d],
S.A. Akimenko[e], A.A. Derevschikov[e], A.S. Konstantinov[e], V.A. Leontiev[e],
Yu.A. Matulenko[e], Yu. Melnick[e], A.P. Meschanin[e], N.E. Mikhalin[e],
N.G. Minaev[e], L.V. Nogach[e], S.B. Nurushev[e], K.E. Shestermanov[e], A.V. Vasiliev[e],
A.E. Yakutin[e], F. Bieser[f], J.B. Carroll[f], H. Chen[f], K. Filimonov[f], B. Holmes[f],
J. Hunter[f], R. Jared[f], J. Klay[f], B. Krieger[f], T. Merrick[f], J. Marx[f], R. Minor[f],
G. Risk[f], P. Salz[f], C. Vu[f], M.B. Tonjes[g], A.M. Vander Molen[g], G.D. Westfall[g],
S. Heppelmann[h], A. Ogawa[h], G. Eppley[i], W. Llope[i], E. Platner[i], V. Ghazikhanian[j],
G.J. Igo[j], S. Trentalange[j], O.D. Tsai[j], C. Whitten[j], N.I. Belikov[k], S. Bennett[k],
A. Bordiukov[k], S. Chattopadhyay[k], T.M. Cormier[k,*], M.M. de Moura[k],
A. Egorov[k], Y. Filippov[k], W. Funk[k], Yu.M. Goncharenko[k,e], O.A. Grachov[k,e],
V. Kormilitsyne[k,e], V. Lavrentiev[k,e], O. Lesovoy[k], Q. Li[k], A.I. Pavlinov[k],
V. Petrov[k,c], I. Pirogov[k], F. Pompei[k], J. Riso[k], V.L. Rykov[k], G. Shamsoutdinov[k],
A.V. Stolpovsky[k], A.A.P. Suaide[k], A. Vilkov[k], S.A. Voloshin[k], Q. Wang[k]

[a] *Argonne National Laboratory, High Energy Physics Division, Argonne, IL 60439, USA*
[b] *Brookhaven National Laboratory, Physics Division, Upton, NY 11973, USA*
[c] *Laboratory of Particle Physics, JINR, Dubna 141980, Russia*
[d] *Indiana University Cyclotron Facility, Bloomington, IN 47408, USA*
[e] *Institute for High Energy Physics, Protvino 142284, Russia*
[f] *Lawrence Berkeley National Laboratory, Berkeley, CA 94720, USA*
[g] *Department of Physics, Michigan State University, East Lansing, MI 48824, USA*
[h] *Department of Physics, Pennsylvania State University, University Park, PA 16802, USA*
[i] *Department of Physics, Rice University, Houston, TX 77251, USA*
[j] *Department of Physics, University of California, Los Angeles, CA 90095, USA*
[k] *Department of Physics, Wayne State University, Detroit, MI 48201, USA*

*Corresponding author.
E-mail address: cormier@physics.wayne.edu (T.M. Cormier).

Abstract

Details concerning the design, fabrication and performance of the STAR Barrel Electromagnetic Calorimeter are presented.
© 2002 Published by Elsevier Science B.V.

1. Introduction

This article describes the STAR Barrel Electromagnetic Calorimeter (BEMC). The detector is among the first significant upgrades to the STAR baseline detector system and will be installed in stages with the first $\approx 25\%$ of the detector installed and ready to operate for the 2001 run. The balance of the STAR BEMC will be completed and installed at a rate of approximately 25% per year. STAR, which is nominally a slow detector, utilizes the BEMC to trigger on and study rare, high P_T processes (jets, leading hadrons, direct photons, heavy quarks) and provide large acceptance for photons, electrons, π^0 and η mesons in systems spanning polarized pp through AuAu collisions. Other applications include general event characterization in heavy ion collisions including ultra-peripheral collisions.

In the following pages, we give an overview of the calorimeter technology and basic layout, followed by the details of various calorimeter subsystems. We conclude with some examples of the calorimeter performance.

2. Technology choices

The total area that must be covered outside the STAR TPC is over $60\,\mathrm{m}^2$ for pseudo-rapidity $|\eta| < 1$. Consequently, cost is a primary consideration in the technology choice implemented in the STAR BEMC. To accomplish all the physics goals, including adequately containing 60 GeV electromagnetic showers, and to satisfy all of the mechanical constraints of the STAR detector, the calorimeter has a total depth of approximately 20 radiation lengths ($20X_0$) at $\eta = 0$.

Because of the large area and complex geometry, a sampling calorimeter using lead and plastic scintillator has been chosen for the detection of electromagnetic energy in STAR. A significant advantage of this technology is that the calorimeter can be constructed from a number of relatively small modules. This approach has permitted the calorimeter to be constructed and installed after the STAR baseline components (TPC, magnet, etc.) are complete. Calorimeters of this design have been successful in a number of colliding beam and fixed target experiments, and as a consequence, the technology is well known [1]. In the present case, in particular, the use of a lead-scintillating sampling calorimeter is a cost effective way to cover the necessary area, employing a mechanical design flexible enough to accommodate the constraints imposed by the closed STAR geometry.

Space constraints also drive the choice of photon transport and detection. With a scintillation light detection scheme utilizing photomultiplier tubes (PMT) and given the space allocated to the BEMC within the STAR magnet, it becomes essential to transport all of the scintillation light outside of the confines of the magnet steel to find sufficient space to accommodate the phototubes, bases, HV system and front end electronics. While this considerably complicates the calorimeter's optical system, it comes with the added advantage that the phototubes can be operated in a near zero magnetic field environment which considerably reduces the PMT system cost and complexity. The use of waveshifter plates and bars to transport the scintillation light outside the STAR magnet, such as those used in the CDF and ZEUS calorimeters, would not be practical in the present application because they would take up an unacceptable amount of space in traversing the large room-temperature solenoidal magnet's coil pancakes and iron flux return path. Consequently, similar to the method developed for CDF [2], a combination of

plastic wavelength shifting and clear optical fibers that take up much less space and require far less labor to prepare has been selected for the STAR design.

Again, because of the large surface area of the STAR electromagnetic calorimeter, it is impractical to choose an independent tower size comparable to the Moliere radius in the lead/scintillator composite material. On the other hand , the STAR physics program requires that the calorimeter permit the reconstruction of the π^0's and isolated (direct) photons at relatively high $P_T \approx 25$–$30\ \mathrm{GeV}/c$ and be capable of identifying single electrons and pairs in intense hadron backgrounds from heavy vector mesons and W and Z decays. All of these measurements require precise electromagnetic shower reconstruction with high spatial resolution. We have chosen therefore to implement shower maximum detectors (essentially two layers of gas wire pad chambers) within the BEMC lead/scintillator stack to provide the high spatial resolution measurements of shower distributions in two mutually orthogonal transverse dimensions. Using shower maximum detector technology, the calorimeter tower sizes need only be chosen small enough to produce reasonable particle occupancies in typical events of interest.

Finally, even the best electromagnetic shower spatial resolution is challenged to distinguish π^0's and γ's for P_T as high as $\approx 25\ \mathrm{GeV}/c$ at the radius of the STAR detector. To facilitate such measurements, an independent preshower detector readout of each tower is provided. These signals provide a measurement of the longitudinal shower development after only $(1-1.5)X_0$ which significantly aids in both π^0/γ and electron/hadron discrimination. At the depth of the preshower detector, there is substantial difference in energy deposition between charged hadrons and electrons. For example, a typical electron exhibits a substantially higher ionization $\mathrm{d}E/\mathrm{d}x$ than hadrons even before the initiation of electromagnetic showers. On top of this, $\approx 63\%$ of electrons will shower before entering the active volume of the preshower and $\approx 84\%$ by the middle of the preshower detector. This is to be compared with the corresponding interaction probability for hadrons of approximately 3% and 6%, respectively. Thus energy distributions for electrons and hadrons differ substantially in the preshower detector in a manner which will be almost independent of energy.

3. The calorimeter mechanical structure

The Barrel Electromagnetic Calorimeter, EMC, is located inside the aluminum coil of the STAR solenoid and covers $|\eta| \leqslant 1.0$ and 2π in azimuth, thus matching the acceptance for full TPC tracking. This is shown schematically in Fig. 1. The front face of the calorimeter is at a radius of $\approx 220\ \mathrm{cm}$ from and parallel to the beam axis.

The design for the Barrel Electromagnetic Calorimeter includes a total of 120 calorimeter modules, each subtending $6°$ in $\Delta\phi$ (~ 0.1 rad) and 1.0 unit in $\Delta\eta$. These modules are mounted 60 in ϕ by 2 in η. Each module is roughly 26 cm wide by 293 cm long with an active depth of 23.5 cm plus about 6.6 cm in structural plates (of which ≈ 1.9 cm lies in front of the detector). The modules are segmented into 40 towers, 2 in ϕ and 20 in η, with each tower subtending 0.05 in $\Delta\phi$ by 0.05 in $\Delta\eta$. The full Barrel Calorimeter is thus physically segmented into a total of 4800 towers, each of which is projective, pointing back to the center of the interaction diamond. Fig. 2 shows a schematic side view of a module illustrating the projective nature of the towers in the η-direction while Fig. 3 shows a photograph of the $\eta = 0$ end of a module after assembly, before the light-tight covers are put in place.

The calorimeter is a sampling calorimeter, and the core of each module consists of a lead-scintillator stack and shower maximum detectors situated approximately 5 radiation lengths from the front of the stack. There are 20 layers of 5 mm thick lead, 19 layers of 5 mm thick scintillator and 2 layers of 6 mm thick scintillator. The latter, thicker scintillator layers are used in the preshower portion of the detector as described below.

The core structure, the stack, is held together by compression that is applied by a combination of 30 straps connecting the non-magnetic front and back-plates of a calorimeter module, and a system of bolts and spring washers between the back plate
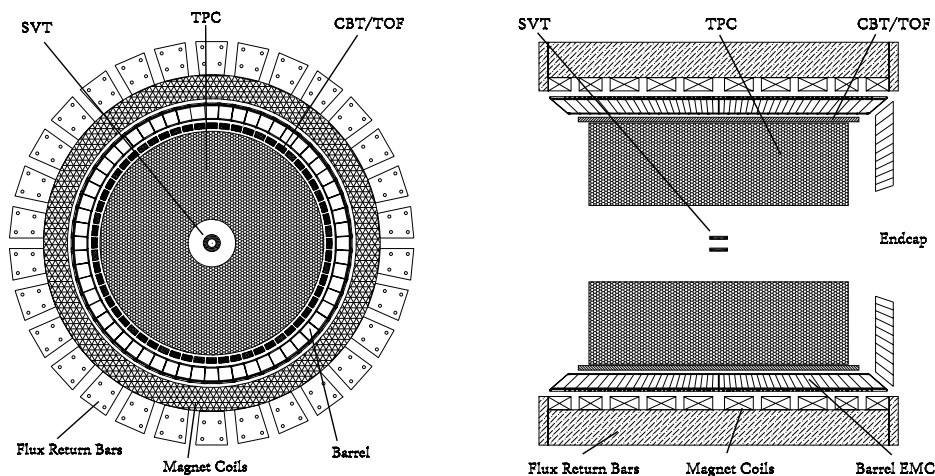
Fig. 1. Cross-sectional views of the STAR detector. The Barrel EMC covers $|\eta| \leqslant 1.00$. The Barrel EMC modules slide in from the ends on rails which are held by aluminum hangers which attach to the magnet iron between the magnet coils. Optical fibers from the towers pass through spaces between the coils and are subsequently routed between the iron flux return bars to the exterior of the magnet.
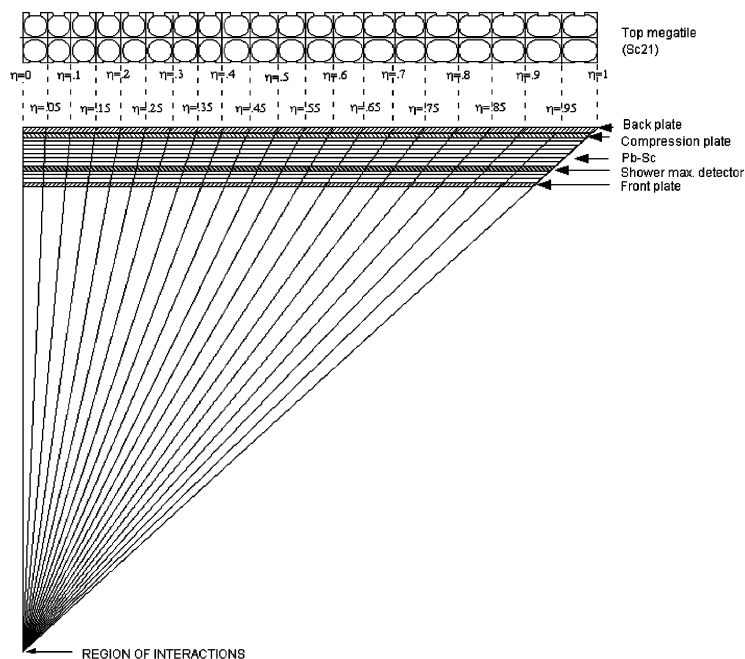

Fig. 2. Side view of a calorimeter module showing the projective nature of the towers. The 21st mega-tile layer is also shown in plan view.

and the compression plate. An average internal pressure is created by this compression system of approximately 15 psi. The stability of the calorimeter stack is guaranteed in any orientation by friction between individual layers. All materials in the stack are chosen to have suitable coefficients of friction.

Fig. 4 shows an end view of a module showing the mounting system and the compression components.
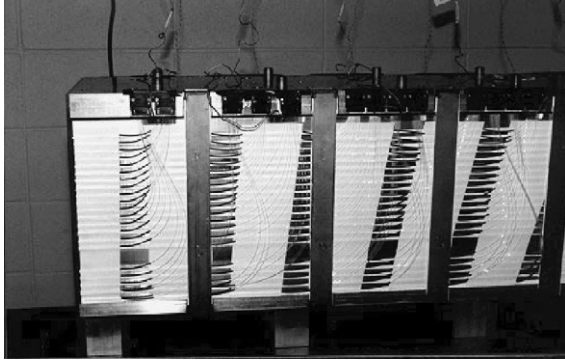
Fig. 3. Photograph of a BEMC module taken near the $\eta = 0$ end showing the projective towers and the WLS fiber routing pattern along the sides of the module. The WLS fibers terminate in 10 pin optical connectors mounted along the back (top in the photo) plate of the module.

4. The STAR BEMC optical structure

There are 21 active scintillating layers in the calorimeter. The material is Kuraray SCSN81 (5 and 6 mm thick). Of these 21 layers, 19 are 5 mm thick and 2, associated with the preshower detector, are 6 mm thick. The scintillator layers alternate with 20 layers of 5 mm thick lead absorber plates. The plastic scintillator is machined in the form of 'megatile' sheets with 40 optically isolated 'tiles' in each layer. The layout of the 21st mega-tile sheet is illustrated in Fig. 2. The signal from each scintillating tile is readout with a wavelength shifting (WLS) fiber embedded in a 'σ-groove' that is machined in the tile. The optical isolation between individual tiles in a given layer is
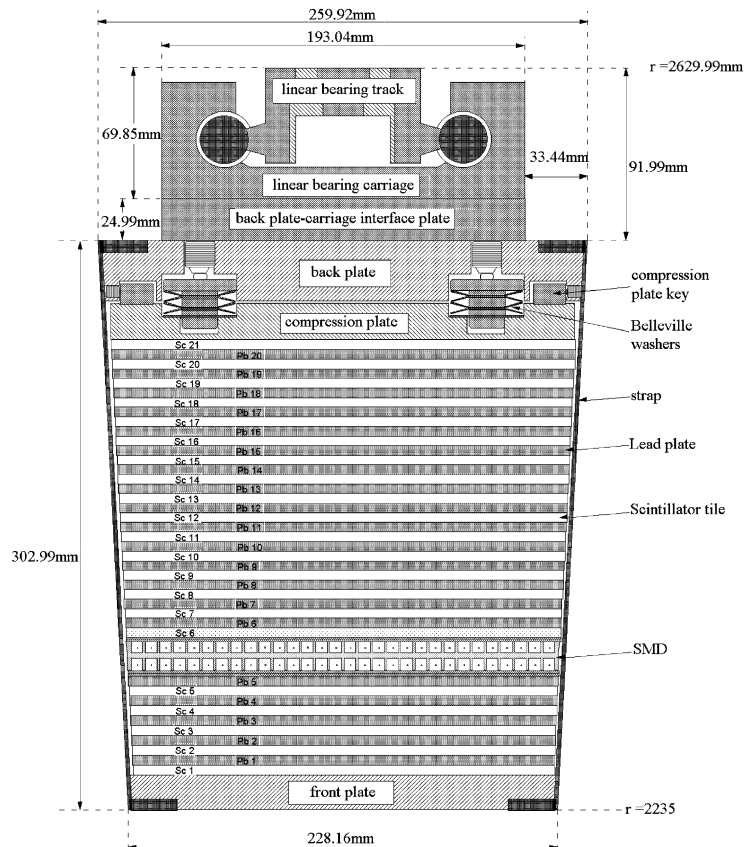

Fig. 4. Side view of a STAR EMC module showing the mechanical assembly including the compression components and the rail mounting system. Shown is the location of the two layers of shower maximum detector at a depth of approximately $5X_0$ from the front face at $\eta = 0$.

achieved by machining 95% of the way through the scintillator sheet and backfilling the resulting groove with opaque, silicon dioxide loaded epoxy. The potential optical cross talk between adjacent tiles as a result of the remaining 5% of the scintillator thickness is canceled to the level of $<\frac{1}{2}\%$ by a thin black line painted at the location of the isolation grooves on the uncut scintillator surface.

A total of 840 different tile shapes (420 plus their mirror image) must be machined in the layers of each module. All this machining is performed on a special high-speed router with two cutting heads operated in parallel which is capable of fabricating two identical mega-tiles simultaneously. Linear cutting speeds approaching 200 in./min are used.

The machined, unpolished mega-tile edges are painted white with Bicron BC620 reflective paint. White bond paper, which has good diffuse reflectivity and most important, a high coefficient of friction, is used on both surfaces of the mega-tile as a diffuse reflector between calorimeter layers.

After exiting the scintillator the WLS fiber are routed along the outer surface of the lead-scintillator stack, under the module's light tight cover, and terminate in a multi-fiber optical connector at the back-plate of the module (Fig. 3). A 2.1 m long multi-fiber optical cable of clear fibers, connected with mating optical connectors, carries the light from the optical connector on the detector through the magnet structure to decoder boxes mounted on the outer surface of the STAR magnet. In these boxes the light from 21 tiles composing a single tower are merged onto a single photomultiplier tube (PMT).

A light mixer is placed between the fibers and the PMT to optimize detection uniformity by insuring that the light from each of the 21 fibers illuminates a common area of the photo-cathode of the PMT. The light mixer used in the PMT housing is made of clear Lucite with dimensions $2'' \times 0.5'' \times 0.5''$. The light mixer design is a compromise between the space constraints of the housing and the mixer functionality based on studies performed at Fermilab [3]. These studies show that the diffusion of light due to the mixer is

optimum for a square rod of length greater than 4 times its transverse dimension. Thus the nominal spatial variation in quantum efficiency across the PMT photo-cathode, which would result in non-uniform response to various tower layers, is reduced to a few percent as a result of utilization of the mixer.

A schematic diagram of the tile/fiber optical readout scheme of the Barrel EMC is shown in Fig. 5.

The WLS fiber used in the BEMC is Kuraray multiclad Y11 (200 ppm) S-type wavelength shifting fiber 0.83 mm in diameter. One end of the wavelength shifting fiber is polished and mirrored with a sputtered aluminum film. The clear fiber used in the 2.1 m cables is Kuraray double-clad 0.9 mm fiber. Kuraray double-clad fiber, 1.0 mm in diameter, is used inside the PMT decoder boxes. Optical connectors are used at each fiber junction where the fiber diameter increases to optimize the optical transfer.

The photomultiplier tubes used for the EMC towers are Electron Tube Inc. model 9125B. These tubes are ≈ 30 mm diameter, 11 dynode, linear-focused PMTs with a photo-cathode sensitive diameter of ≈ 23 mm. A quantum efficiency near 25% at peak sensitivity is typical. PMT's accepted
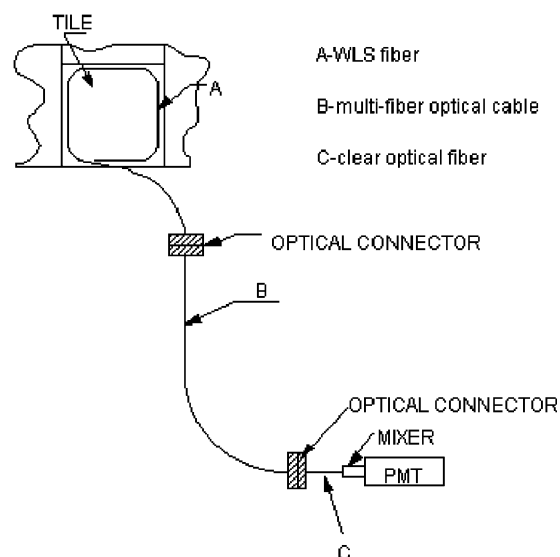

Fig. 5. Schematic diagram of the BEMC optical system illustrated for a single tile.

for use in the BEMC have a mean quantum efficiency of 13.3%, with a standard deviation of 1.3%, at the wavelength delivered by the BEMC fibers. No PMT is used whose quantum efficiency is less than 10% at 490 nm. Additional acceptance criteria include dark current less than 5 nA (at a gain of 2×10^5), and non-linearity of less than 2% at a peak current of 20 mA. The 9125B tube was selected primarily for its linearity, dark current, gain, and quantum efficiency specifications as well as for its lower cost. All PMTs used in the BEMC undergo preliminary factory testing before delivery. Further quality control and characterization tests are performed on the PMTs before final installation in STAR. These tests include gain, dark current, and linearity measurements. An automated test setup has been designed and built to perform these tests.

To achieve the required PMT linearity and noise performance, to meet the STAR safety requirements, to achieve low power operation and to reduce system cost, we have designed and built an intelligent Cockroft Walton PMT base. Each PMT base consists of a Pulse Frequency/Pulse Width Modulation system which generates and regulates the HV within the base. The HV division ratio was optimized for linearity and is 2:1:1:1:1:1:1:1:2:3:4:3 (K:d1:....:d11:A). The PMT bases are controlled by a 8051-compatible flash microcontroller (e.g., Analog Device's ADUC812) with internal 12-bit DAC and ADCs. The HV ripple measured at the photo-cathode with a 1 μA load is 0.05% at 1000 V. The base was optimized so that the injected noise into the anode signal is far below 0.15 pC (one least significant bit (LSB)). The HV range is hardware and firmware limited to −1520 V. The setpoint voltage resolution is 0.6 V with a 0.3% full range accuracy.

The bases' HV are controlled by an RS485 serial network in a master–slave configuration. Each base has a unique 12-bit address; and therefore up to 4096 such bases can be controlled on a single segment of the control network. Due to limitations on the RS485 transceiver, the control signal from the master (i.e., from a PC) needs to be regenerated by an appropriate number of repeaters. (Each PMT box containing 80 PMTs is connected to a repeater.) The slow control software is written in LabView and resides on the master (PC). In addition to measuring HV, the bases are capable of measuring temperature and current, although in the latest hardware revision the current measurement is disabled. More details on the HV system will be presented in a separate publication.

Layer by layer tests of the BEMC optical signal, and full system tests with cosmic rays and test beams, show that an average of 3 photoelectrons per minimum ionizing particle (mip) per calorimeter layer are produced from the fully integrated optical system. For these photostatistics, the resolution of an ideal sampling calorimeter is expected to be $\approx 14\%/\sqrt{E}$ plus a 1.5% constant term added in quadrature. In a real sampling calorimeter, transverse and longitudinal non-uniformities within a tower, and cross talk between towers, are the limitations to achieving this limiting resolution. In the STAR BEMC optical system, design and quality assurance criteria have been imposed to insure that the following limits are not exceeded:

(i) transverse uniformity of the scintillating light from each tile better than 5% RMS;
(ii) longitudinal uniformity to a level of less than 10% RMS within each tower, including all contributions from fiber system variations;
(iii) total optical cross talk less than $\frac{1}{2}$% between adjacent tiles.

Fig. 6 shows the frequency distribution of the relative number of photo-electrons produced from a sample of 160 tiles selected at random from two modules. This sample represents $\approx 10\%$ of all tiles in these modules. The observed RMS variation of 8.1% includes all effects along individual optical chains, from the scintillating tile itself, through to and including the possible non-uniformities in the light distribution after the mixer at the PMT photo-cathode. The measurements have all been made with a single PMT so that tube to tube variations in quantum efficiency do not enter. The later variations are equivalent to an overall channel gain variation and, for the range of quantum efficiencies selected for use in STAR, do not impact a particular tower's resolution.
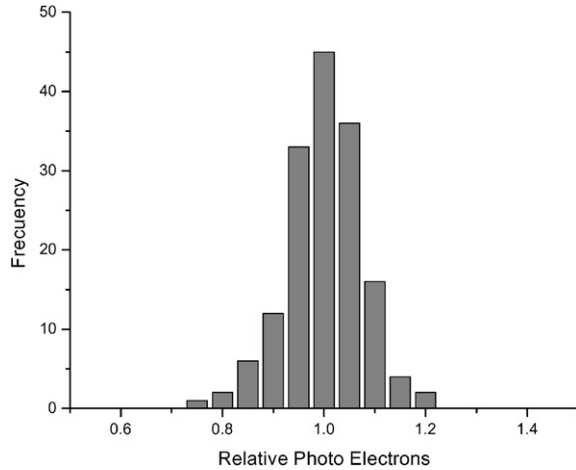
Fig. 6. Relative individual tile photo-electron yield for a sample of 160 tiles from modules 8 and 12. The observed RMS deviation is 8.1%.

5. Shower maximum detector

A shower maximum detector (SMD) is used to provide fine spatial resolution in a calorimeter which has segmentation (towers) significantly larger than an electromagnetic shower size. Each of the 4800 towers of the BEMC span $\Delta\eta \times \Delta\phi = 0.05 \times 0.05$ which at the radius of the inner face of the detector correspond to tower sizes $\sim 10 \times 10$ cm^2 at $\eta = 0$ increasing towards $\eta = 1$. While the BEMC towers provide precise energy measurements for isolated electromagnetic showers, the high spatial resolution provided by the SMD is essential for π^0 reconstruction, direct γ identification, and electron identification. Information on shower position, shape, and from the signal amplitude the electromagnetic shower longitudinal development, are provided.

Fig. 7 shows the conceptual design of the STAR BEMC SMD. It is located at ≈ 5.6 radiation lengths depth in the calorimeter modules, at $\eta = 0$, including all material immediately in front of the calorimeter.[1] A unique feature of the STAR SMD is its double layer design. A two sided aluminum extrusion provides ground channels for two

independent planes of proportional wires. Independent PC Board cathode planes with strips etched in the η- and ϕ-directions, respectively, allow reconstruction of a two-dimensional image of the shower as shown schematically in Fig. 7.

The shower max detector is a wire proportional counter—strip readout detector using gas amplification. The structure is very similar to that used in the CDF Barrel EMC, except for the additional layer of wires with parallel readout strips. These additional strips have lengths chosen to limit occupancy (see below). The basic structure of the detector is an aluminum extrusion with 5.9 mm wide channels running in the η-direction. A cross-sectional view of the detector is shown in Fig. 8 and the design parameters are summarized in Table 1.

There are 50 μm gold-plated tungsten wires in the center of the extrusion channels. The detector strips sense the induced charge from the charge amplification near the wire. One set of strips is perpendicular to the wires, making up one side of the channel around the wire outside the aluminum extrusion, and provide an image of the shower spatial distribution in the η-direction. Each of these strips span 30 channels (30 wires). They have size of 0.1 rad in ϕ (≈ 23 cm, i.e. the module width) and 0.0064 in η (≈ 1.5 cm at low η). The other set of strips are parallel to the wire channels of the aluminum extrusion. These strips are physically 1.33 cm wide and have lengths 0.1 units in η, while the wires are 1.0 units in η.

Some important features of the double sided SMD design include improved reliability, improved functionality in a high occupancy environments, improved hadron rejection and π^0/γ separation, and simplified mechanical construction. The later point is particularly significant. Single sided aluminum extrusions of the length used in the STAR SMD are notoriously difficult to produce sufficiently flat and straight for our application. The double sided extrusion design, in addition, made it easy to satisfy the mechanical constraints for insertion within the EMC stack.

There are a total of 36 000 strips in the full detector and 120 ganged wire channels in the full Barrel Calorimeter. Each of the 1200 distinct areas, approximately 0.1 by 0.1 in η–ϕ, has 15 ϕ

---

[1] The depth of the shower maximum detector varies from $4.6X_0$ to $7.1X_0$, counting only the calorimeter material, as η varies from 0 to 1.
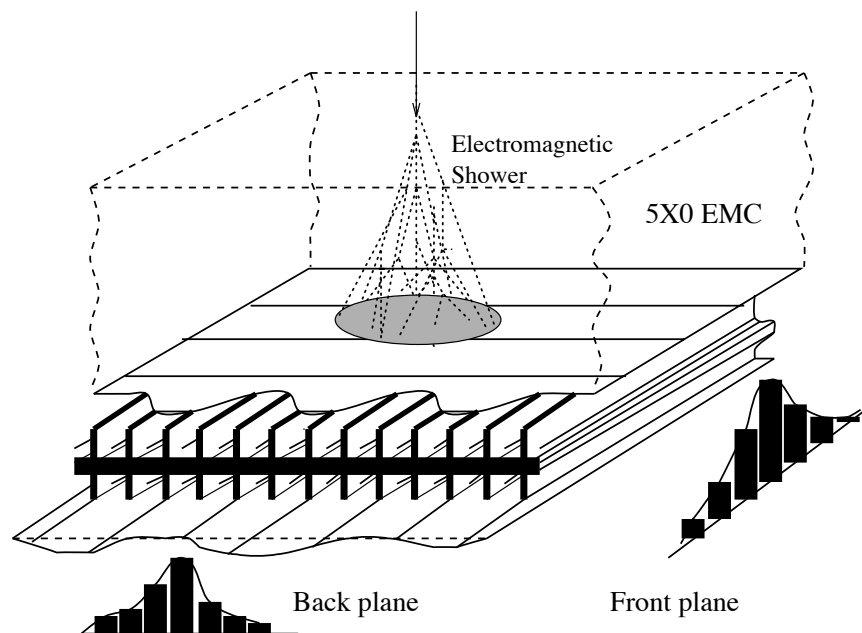
Fig. 7. Schematic illustration of the double layer STAR BEMC SMD. Two independent wire layers, separated by an aluminum extrusion, image electromagnetic showers in the η- and ϕ-directions on corresponding pad layers.
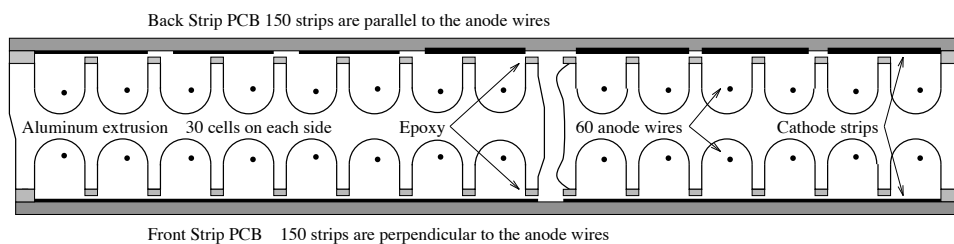

Fig. 8. Cross-sectional view of the SMD showing the extruded aluminum profile, the wires and cathode strips.

strips and 15 η strips. The wires in the shower maximum detector in each of the 120 EMC modules have a length 1.0 in η. Signals from the wires can be used to provide 120 independent shower max trigger signals from the Barrel EMC, each spanning $\Delta\eta \times \Delta\phi = 1.0 \times 0.1$. Because the detector is inside the lead scintillator stack, the SMD is under a fixed pressure of 15 psi.

The signal size of the SMD strips is less than ≈ 7 fC/mip. The interior of the STAR magnet is a potentially noisy environment where the voltage ripple on the face of the magnet coils could be as large as 400 V with no filtering. In order to preserve the small SMD signals and to have the required $\approx 1:1000$ dynamic range for analog

signals, there is a front end electronics (FEE) board mounted at the $\eta = 1$ end of each module. Signals from the cathode propagate along a transmission line plane in the printed circuit boards to reach the FEE mother board. This transmission line plane is located between the plane of cathode strips themselves and a full ground plane which forms part of the outer enclosure of the detector. The strip lines themselves are spaced to achieve reasonable strip-to-strip cross-capacitance, low fabrication cost and a minimum number of manufacturing steps in the final assembly. At the FEE board, the amplified cathode strip signals are buffered in a switched capacitor array before being multiplexed 80:1 to

Table 1
SMD design parameters

Chamber depth inside EMC	$\sim 5X_0$ at $\eta = 0$
Rapidity coverage (single module)	$\Delta\eta = 1.0$
Azimuthal coverage (single module)	$\Delta\phi = 0.105$ R $(6°)$
Occupancy (p + p)	$\approx 1\%$
Occupancy (AuAu)	> 5 to $\approx 25\%$ (depends on threshold cut)
Chamber depth (cathode to cathode)	20.6 mm
Anode wire diameter	50 μm
Gas mixture	90%-Ar/10%-CO_2
Gas amplification	≈ 3000
Signal length	110 ns
Strip width (pitch) in η for $|\eta| < 0.5$	1.46 (1.54) cm
Strip width (pitch) in η for $|\eta| > 0.5$	1.88 (1.96) cm
Strip width (pitch) in ϕ	1.33 (1.49) cm
Number of strips per module	300
Total number of modules	120
Total number of readout channels	36 000

external digitizers mounted outside the STAR magnet. The amplifier used on the FEE board is essentially the same as that employed in the STAR TPC with the ASIC modified to set the sensitivity to match the larger SMD dynamic range. The shaping time at the amplifier and the reset time at the integrator were optimized for the SMD using actual experiment pulse shapes obtained from radioactive sources. The combined uniformity of the SMD and its FEE system is expected to be at the level of $\pm 14\%$ before any calibration and the channel to channel cross talk should not exceed 1%.

The SMD has been extensively evaluated in test beams at the AGS. In the energy range from 0.5 to 5 GeV, at a depth of $5X_0$ inside the EMC, the SMD has an approximately linear response versus energy. The ionization at the back plane of the SMD is about 10% lower than the front plane. The energy resolution in the front plane is given approximately by $\sigma/E = 12\% + 86\%/\sqrt{E}$ [GeV] with the energy resolution on the back plane being 3–4% worse. The position resolution in the front and back planes of the SMD have been measured in test beams. We find the resolution in the front and back planes are given approximately by

$$\sigma_{\text{front}} \text{ (mm)} = 2.4 \text{ mm} + 5.6 \text{ mm}/\sqrt{E} \text{ [GeV]}$$

and

$$\sigma_{\text{back}} \text{ (mm)} = 3.2 \text{ mm} + 5.8 \text{ mm}/\sqrt{E} \text{ [GeV]}.$$

The systematic difference in performance of the front and back planes has been discussed in a previous publication [4].

6. Preshower detector

A preshower detector is integrated into each of the 4800 towers of the BEMC. The first and second scintillating layers of the calorimeter comprise the preshower detector. To accomplish this, the fiber readout grooves are cut somewhat deeper into the mega-tile and two WLS fibers are inserted to bring two samples of the scintillation light from these two layers out to the PMT/Decoder boxes. The first pair of fibers from layers 1 and 2 merge with 19 other tower fibers to produce the total energy signal. The second pair of fibers illuminate a single pixel of a multi-anode PMT. A total of 300, 16 pixel multi-anode PMTs are used to accommodate the 4800 fiber pairs providing the tower preshower signals.

By placing two fibers in a single readout groove, we find that the light delivered by each fiber is reduced by 20% compared to that of a single fiber. While this is of no significant concern for the preshower signal, it would cause layers 1 and 2 of each tower to be out of the 10% tolerance set for the longitudinal uniformity for the tower as a whole. To compensate for this, we use 6 mm thick scintillator for layers 1 and 2.

7. Summary of BEMC electronics systems

The EMC electronics includes trigger, readout of phototubes and SMD, high-voltage system for phototubes, low voltage power, slow controls functions, calibration controls, and interfaces to the STAR trigger, DAQ and slow controls. The bulk of the front end electronics including signal processing, digitization, buffering, formation of trigger primitives, and the first level of readout is located in custom EMC crates on the outside of the magnet iron. The exception is the preamplifiers

and switched capacitor array's which form the analog pipeline for the SMD wire chambers. They reside on the EMC modules inside the STAR magnet.

In STAR's trigger hierarchy, level-0 consists of that detector information available, without dead time, at each RHIC crossing. Level-0 is distinct from all higher levels in that level-0 selects events for processing while all other trigger levels only function as event aborts. The BEMC uses gated integrators and 12-bit flash ADCs along with a long digital pipeline to insure deadtimeless operation at the RHIC clock frequency. In this way, the BEMC functions as an important part of STARs level-0 trigger, capable of triggering on high-P_T physics through its electromagnetic component. For example, the STAR jet trigger relies largely on leading π^0's in the BEMC with some contribution from the significantly smaller energy deposition of hadronic showers, to form level-0 jet triggers. Additional jet trigger information at level-0 comes from STAR's multiplicity detectors.

In STAR, the level-0 trigger is the only level which does not incur large dead times from the opening of the gated grid in the TPC. For all practical purposes, as noted, level-0 is deadtimeless and capable of action on each RHIC beam crossing. The TPC grid cycling rate is limited which makes it very important to concentrate as much functionality as possible in level-0 trigger. The EMC is an important detector for STARs level-0 because it is fast and it is sensitive to the particles' total energy. The STAR level-0 trigger must ultimately provide a trigger to the TPC within about 1 μs ($\sim$ 10 RHIC crossings) and to the STAR level-0 trigger processors within about 700 ns, including cable delays. For reasons of speed and limited bandwidth, the EMC trigger uses trigger primitives instead of the full EMC data. There are two kinds of trigger primitives from the EMC front end electronics. The first set of primitives is 300 tower sums, digitized to 6 bits each, from patches of 0.2 by 0.2 in $\eta-\phi$. The second is 300 high tower values of 6 bits from the single largest 0.05×0.05 tower signal within each 0.2×0.2 patch. These primitives are processed to make final trigger decisions based on total E_T, jet triggers, photon triggers, etc. These results are

then passed to STAR level-0 in 700 ns to participate as a component of the final level-0 decision.

The BEMC tower data are processed via a separate path. The phototube signals from the towers are integrated and digitized in the front-end cards on every RHIC crossing. These data are pipelined until level-0 trigger time, and if a trigger occurs they are transferred to a token-addressable memory in the tower data collector located on the STAR electronics platform to await readout. The signals from the pads of the SMD are amplified with a simple transimpedance amplifier and driver on the front end processing cards before entering an analog pipeline composed of switched capacitor arrays to await the level-0 trigger. Upon level-0 trigger, the SMD analog signals are queued with multiplexing ratio of 80:1 to the 10-bit SMD digitizers. SMD digitized signals are first available in STAR's level-2 trigger processors in $\sim$ 200 μs, still well ahead of digital information from the TPC.

8. BEMC performance estimates

Finally, as an example of BEMC performance in STAR, we focus on electron–hadron discrimination in the energy range encountered in AuAu collisions, 500 MeV to 5 GeV. STAR, with its very large acceptance and event-by-event capability will be an important tool in the study of vector meson production and suppression in heavy ion collisions at RHIC, provided adequate electron identification and hadron suppression can be achieved. In both cases of immediate interest, $\phi \rightarrow e^+e^-$ and J/ψ, electron spectra must be observed against an overwhelmingly more intense hadron background. The efficiency of electron identification and the corresponding hadron rejection factor thus strongly influence the phase space for these particles and other lepton channels in STAR. Difficult as these measurements will be, however, they provide direct insight into matters central to the physics of the quark-gluon plasma.

Here we focus on relatively low-energy electrons because this region is most relevant to the RHIC

heavy ion program and because it presents the most challenging hadronic background. This focus, however, is not meant to imply that the BEMC is limited to this relatively low energy regime. Indeed, the BEMC is the central tool in STAR's spin physics program where electrons from W and Z decay and Drell–Yan pairs will be studied to probe, among other things, the sea quark polarization in the proton.

The emphasis of the present study, however, was to provide better estimates of the ability of the STAR detector with the BEMC to provide electron identification in the low-energy region (0.5–5.0 GeV) most relevant in the study of J/ψ and perhaps $\phi \rightarrow e^+e^-$ at low P_T in AuAu collisions. In particular, electron–hadron discrimination has been studied with experimental data obtained in a 1998 EMC test beam run and extended with simulations of the Electromagnetic Calorimeter, including the preshower detector (PSD) and shower maximum detector elements. Other detector elements in STAR beyond the scope of the present study, in particular the Time of Flight (TOF) and RICH detectors as well as TPC dE/dx, can also contribute significantly to electron identification. Unfortunately, both TOF and RICH have acceptances that will be too small, at least initially, to contribute significantly to vector meson studies, although they will provide important extensions to STAR's particle identification capabilities for more abundant particles. TPC dE/dx information, on the other hand, will make a significant contribution to electron identification both in the relativistic rise region and below about 300–400 MeV where pions begin to have β significantly different from one (> 5% at 400 MeV). This additional capability, which comes with STAR's full acceptance, can be combined with the BEMC's hadron suppression studied here. In vector meson invariant mass spectra, each additional independent contribution to the hadron suppression enters squared.

The mean hadronic background energy in any given BEMC tower in a central AuAu event is on the order of 140 MeV/tower with a standard deviation of 170 MeV. For the J/ψ program considered in this section, a minimum electron energy of 1.5 GeV is imposed for which the intrinsic resolution of the calorimeter is $\sigma_E/E = 12\%$ or ~ 180 MeV.

Effectively, the underlying AuAu event degrades the calorimeter resolution to 17% at 1.5 GeV for the most central events. By an electron energy of 3 GeV the impact of the underlying central AuAu event has decreased, effectively degrading the calorimeter resolution, from 9% to 10%. Although we will not discuss it in this document, the average background energy can be significantly reduced below these nominal levels even by very modest isolation cuts using TPC tracking and the shower maximum detector.

In the present analysis, we consider all of the information potentially available from the EMC towers, the SMD and the PSD. The following eight parameters are considered: E/p, $E_{SMD}(\eta)$, $E_{SMD}(\phi)$, $\Delta\eta$, $\Delta\phi$, σ_η, σ_ϕ and E_{PSD}.

1. E/p: The EMC tower energy provides a high resolution, linear measure of the full energy of electrons that strike it. Hadrons, on the average, even those which shower within the calorimeter, typically deposit far less than their total energy in a tower. A comparison of tower energy to tracked momentum, E/p, thus is an electron identifier whose effectiveness varies with the momentum resolution of the TPC and the calorimeter's energy resolution. The latter scales as $\propto 1/\sqrt{E}$ and thus E/p electron selection improves with increasing energy until dominated by the TPC resolution at higher P_T.

2. E_{SMD}, shower maximum detector energy deposition: The SMD is located within the calorimeter at a depth of approximately 5.6 radiation lengths. This number includes the calorimeter itself plus other material directly in front of the calorimeter. At this depth, the SMD is near the maximum density of electromagnetic showers with energies greater than about 1–2 GeV whereas hadronic showers have maximum density of energy deposition near one interaction length (e.g., 17 cm for Pb) and exhibit a much broader longitudinal distribution. This distinction renders the energy deposition in the shower maximum detector compared to the total energy deposited in the tower useful for hadron

suppression. The electromagnetic shower maximum depth varies logarithmically with energy and consequently this signal is useful over a very wide energy range > 1–2 GeV. At lower energies, < 1 GeV, the shower depth quickly becomes less than $5.6X_0$ and the SMD contributes little to electron discrimination. Hadrons which pass a SMD cut tend to be those for which hadronic showers occur early in the detector and particularly those which produce leading π^0's. Consequently, hadrons which pass an SMD cut tend to be those depositing a larger than average fraction of their total energy in the calorimeter and are therefore those that are most difficult to remove with the E/p cut. This is an example of the kind of correlations that render combined detectors less effective than the simple product of their individual hadron rejection powers. There are two SMD layers $E_{SMD}(\eta)$ and $E_{SMD}(\phi)$. While these signals are strongly correlated on the average, their instrumental fluctuations are far less so and preliminary experimental studies have shown that there is a significant advantage to including both $E_{SMD}(\eta)$ and $E_{SMD}(\phi)$ in the analysis.

3. $\Delta\eta, \Delta\phi$, shower position: For charged particles, TPC tracking determines the expected hit position at the calorimeter with mm-like precision. The response of the shower maximum detector is used to reconstruct the hit position in the η- and ϕ-directions from the centroids of the measured transverse shower distributions. Hadronic showers, which are typically incompletely developed by the $5.6X_0$ depth of the SMD, show centroids of energy deposition which can fluctuate substantially with respect to the extrapolated track position from the TPC. Thus the measured errors in the reconstructed versus extrapolated hit positions, $\Delta\eta, \Delta\phi$, can be used to provide additional hadron suppression in the energy range where good SMD signals are observed, typically > 1 GeV.

4. σ_η, σ_ϕ, shower shape: Electromagnetic showers exhibit compact shapes with $\sim 95\%$ of the shower energy contained in a cylinder of radius equal to twice the Moliere radius (e.g., $2R_M = 3.2$ cm for Pb). On the other hand, the transverse dimensions of hadronic showers are much larger, approximately one interaction length, λ, when

fully developed (at depth $\sim \lambda$). At the SMD depth, incompletely developed hadronic shower transverse dimensions exhibit substantial fluctuations, but may still be significantly larger than corresponding electromagnetic showers. Thus the standard deviations of the observed shower distributions in the η- and ϕ-directions, σ_η, σ_ϕ, reconstructed from the measured shower profiles in the SMD, are expected to contribute to hadron suppression, again, for electron energies approximately > 1 GeV.

5. E_{PSD}, preshower detector energy deposition: The first and second scintillating layers of the calorimeter comprise the preshower detector. A typical electron exhibits a substantially higher dE/dx than hadrons, even before the initiation of an electromagnetic shower, and $\sim 63\%$ of electrons will shower before scintillator layer 1 and $\sim 84\%$ before layer 2. This is to be compared with the interaction probability for hadrons (considering only the Pb) of approximately 3% before the first layer and 6% before the second layer. Thus, energy distributions for electrons and hadrons differ substantially in the preshower detector in a manner which will be almost independent of energy. Consequently, the preshower detector is particularly important to the overall hadron suppression at energies near 1.5 GeV where the SMD is becoming less useful. At all energies, however, the low hadronic interaction lengths which proceed the preshower detector cause it to be substantially uncorrelated with the other hadron suppressing signals and therefore to contribute, for constant electron detection efficiency, a nearly constant hadron suppression.

Each of the signals described above is correlated to a greater or lesser degree with the others and, furthermore, the extent of the correlation between any two signals may vary with energy. To correctly account for these correlations in an analysis of electron–hadron discrimination, a simultaneous analysis of all signals is required. Furthermore, to ascertain the contribution of any one signal to the overall hadron suppression, one must compare the hadron suppression achieved with all signals utilized, to that achieved when the detector in question is removed from the analysis. For these

reasons, a neural network analysis of the detector signals for hadrons and electrons has been chosen. In this way one can calculate the correlation corrected contribution of any single (or any group of) signal (s) by removing the signal or signals in question and retraining the network. To investigate this type of calculation, we have chosen to apply a neural network analysis of GSTAR simulated data in which a seven node network ($E_{SMD}(\eta)$ and $E_{SMD}(\phi)$ are not treated separately in this first analysis) is trained to distinguish electrons and hadrons. Our sample data sets consisted of pure π^+ or e^+ at momenta of 0.5, 1.0, 2.0 and 5.0 GeV/c. Electron statistics were typically 1000 and hadron statistics were typically 5000 events.

For both the tower energy and preshower energy depositions, ADC channels were computed using the measured photo-electron yields of 3 photo-electrons per MeV of energy deposition and were smeared with a realistic simulation of the photomultiplier single photo-electron response. This latter effect is particularly important for the preshower detector where the mean signal for a minimum ionizing particle produces just 8 photo-electrons from the two layers of the preshower detector combined. At present, in the absence of a good model for the full system response of the shower maximum detector, we work directly with GEANT energy depositions. Electronic noise is expected to degrade the performance of the shower maximum detector only at the very lowest energies where, in any event, the preshower detector is more important. The momentum of the incident particle is smeared by an amount consistent with the expected performance of the STAR TPC, before using it in relation to the measured calorimeter energy to produce a "measured" E/p parameter. Fig. 9 shows the output of the neural network for 1.0 GeV/c electrons and hadrons. The network has been trained such that hadrons produce the maximum near $\alpha = 0$ and electrons near $\alpha = 1$. Given this plot at each energy, the effectiveness of electron–hadron discrimination can be characterized by the hadron efficiency ε_h and the electron efficiency ε_e obtained by integrating data such as in Fig. 2 over the appropriate interval of α from some α_{cut} to $\alpha = 1$. As α_{cut} is
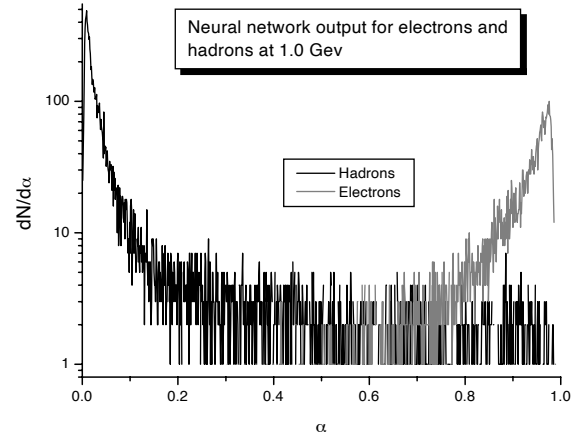

Fig. 9. Output of the seven node neural network as trained for 1 GeV/c electrons and 1 GeV/c hadrons. The data sample contained 5000 hadrons and 1000 electrons.
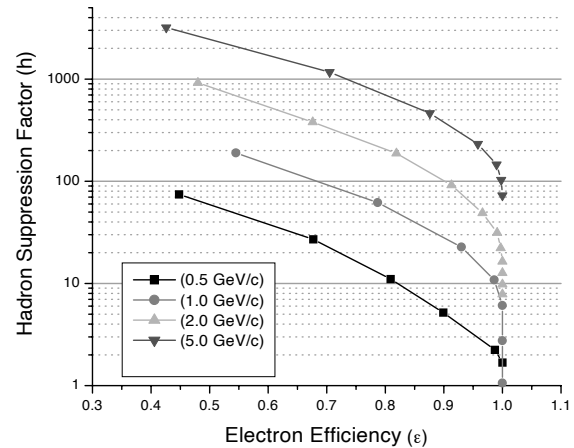

Fig. 10. Hadron suppression factors, h, for various electron energies as a function of electron detection efficiency.

varied, the functional dependence of ε_h on ε_e is determined. The hadron suppression factor, $h = 1/\varepsilon_h$ computed in this manner at each corresponding electron efficiency is shown in Fig. 10 for 0.5, 1.0, 2.0 and 5.0 GeV/c, respectively. Roughly speaking, the signal to background ratio for a single electron measurement is $(M_e/M_h)(\varepsilon_e/\varepsilon_h)$ where M_e and M_h are the electron and hadron multiplicities.

9. Conclusions

We have described the STAR Barrel Electromagnetic Calorimeter. This detector, which is among the first significant upgrades to the STAR baseline detector system is being produced and installed in stages with the first $\sim 25\%$ of the detector installed and ready to operate for the 2001 run. With an acceptance equal to that of the TPC for full length tracks, the BEMC allows STAR to trigger on and study rare, high P_T processes (jets, leading hadrons, direct photons, heavy quarks) and provide large acceptance for photons, electrons, π^0 and η mesons in systems spanning polarized pp through AuAu collisions.

References

[1] G.W. Foster, J. Freeman, R. Hangstrom, Nucl. Phys. B A 23 (1991) 93;
    P. de Barbaro, et al., Nucl. Instr. and Meth. A 315 (1992) 317.
[2] S. Kim, Nucl. Instr. and Meth. A 360 (1995) 206.
[3] W. Koksa, et al., Light mixer studies, Fermilab Report TS-DET 93-038.
[4] S. Akimenko, et al., Nucl. Instr. and Meth. A 365 (1995) 92.